Applied Surface Science 257 (2011) 7837–7844

Contents lists available at ScienceDirect

Applied Surface Science

journal homepage: www.elsevier.com/locate/apsusc

Nitrogen-doped carbon nanotubes with tunable structure and high yield produced by ultrasonic spray pyrolysis

Jian Liu, Yong Zhang, Mihnea Ioan Ionescu, Ruying Li, Xueliang Sun*

Department of Mechanical and Materials Engineering, University of Western Ontario, London, ON, Canada N6A 5B9

ARTICLE INFO

Article history:
Received 28 March 2011
Received in revised form 7 April 2011
Accepted 7 April 2011
Available online 15 April 2011

Keywords:
Carbon nanotubes
Spray pyrolysis
Nitrogen doping
Chemical vapor deposition

ABSTRACT

Nitrogen-doped carbon nanotubes (CN_x) were prepared by ultrasonic spray pyrolysis from mixtures of imidazole and acetonitrile. Imidazole, as an additive, was used to control the structure and nitrogen doping in CN_x by adjusting its concentration in the mixtures. Scanning electron microscopy observation showed that the addition of imidazole increased the nanotube growth rate and yield, while decreased the nanotube diameter. Transmission electron microscopy study indicated that the addition of imidazole promoted the formation of a dense bamboo-like structure in CN_x. X-ray photoelectron spectroscopy analysis demonstrated that the nitrogen content varied from 3.2 to 5.2 at.% in CN_x obtained with different imidazole concentrations. Raman spectra study showed that the intensity ratio of D to G bands gradually increased, while that of 2D to G bands decreased, due to increasing imidazole concentration. The yield of CN_x made from mixtures of imidazole and acetonitrile can reach 192 mg in 24 min, which is 15 times that of CN_x prepared from only acetonitrile. The aligned CN_x, with controlled nitrogen doping, tunable structure and high yield, may find applications in developing non-noble catalysts and novel catalyst supports for fuel cells.

1. Introduction

Over the last decade, carbon nanotubes (CNTs) [1] have been widely studied due to their unique properties and potential applications in various fields, such as electronics, optics and energy conversion [2,3]. Depending on the requirement of different applications, the properties of CNTs can be modified through different functionalization methods, of which doping foreign elements is an effective and frequently used approach [4]. Due to its similar atomic size with carbon, nitrogen (N) is widely studied as a doping element in CNTs. It is revealed that the incorporation of N could change the nanotube structure [5], chemical reactivity [6], electrical conductivity [7,8], and mechanical properties [9] of CNTs. Due to the tunability of these properties, nitrogen-doped carbon nanotubes (CN_x) have shown promising application potentials in various fields. For example, Dai and co-workers [10] have reported that aligned CN_x could provide high electrocatalytic activity for oxygen reduction reactions (ORR) in fuel cells as a metal-free electrode. It has been found that the field emission property of CNTs could not only be improved by N doping [11], but also be tailored by controlling the graphitic/pyridinic N substitution [12]. In addition, uniform and dense Pt nanoparticles have been achieved by using CN_x as substrates [13,14]. The CN_x supported Pt nanoparticles exhibit greatly improved stability [13] and electrocatalytic activity [14] for ORR in proton-exchange membrane fuel cells, compared with Pt nanoparticles supported on regular CNTs.

Recently, the doping techniques, especially in a controllable manner, have been widely studied. Various synthesis methods have been developed to produce CN_x, including arc discharge [15], laser ablation [16], and chemical vapor deposition (CVD) [17]. The CVD method has been proven to be more controllable and more cost effective than the others. However, the practical application of CN_x requires the production of fairly large amounts of high-quality CN_x at a commercially viable price. Among various CVD based techniques, spray pyrolysis and aerosol assisted CVD (AACVD) seem to be suitable methods for industrial scale production of CN_x. For example, both methods allow continuous injection of carbon and catalyst precursors, and require no additional catalyst preparation step [18,19]. Using these two methods, it is possible to produce CN_x without any flammable or corrosive gases such as hydrogen and ammonia [18]. Looking at these two methods, one can find that spray pyrolysis can spray solution directly into the synthesis system at controlled flow rates [18], whereas AACVD can generate solution droplets with controlled sizes [19]. Nevertheless, these desirable features have not been realized in one setup till now. Herein, by combining the advantages of spray pyrolysis and AACVD, we designed an improved spray pyrolysis method, called *ultrasonic spray pyrolysis*. In ultra-

* Corresponding author. Tel.: +1 519 661 2111x87759; fax: +1 519 661 3020.
E-mail address: xsun@eng.uwo.ca (X. Sun).

0169-4332/$ – see front matter © 2011 Elsevier B.V. All rights reserved.
doi:10.1016/j.apsusc.2011.04.041

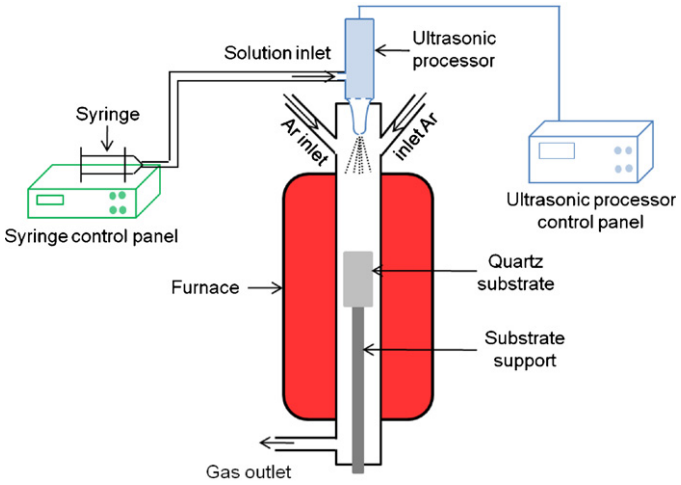

Fig. 1. Schematic illustration of ultrasonic spray pyrolysis.

sonic spray pyrolysis, an ultrasonic processor is used to generate fine solution droplets, which are directly sprayed into the synthesis system at controlled flow rates. Moreover, ultrasonic spray pyrolysis also features several other advantages including: (1) no need for preformed substrates; (2) possible use of mixtures of solid and liquid precursors; (3) easy scaling into an industrial scale process.

Besides the synthesis method, the controllable doping of N in CNTs also relies on the choice of precursor, catalyst, reaction temperature, reaction time and gas flow rate [20–24]. Recently, some interesting progress has been made in controlling the morphology and structure of CN_x by using different liquid N precursors [21–23]. For example, a CNT array doped with a gradient of N concentration was achieved by gradually increasing the pyridine concentration in xylene [21]. Koós et al. reported that CN_x with different structures were prepared by using the mixture of benzylamine and toluene [22,23]. It was found that bamboo shaped nanotubes increased with the increase of benzylamine concentration, but the length and diameter of the nanotubes decreased dramatically [22,23]. In those studies, controlled doping of N in CNTs was realized by adjusting the concentration of the N-containing precursor in the N-free precursor. However, the involvement of the N-free precursor inevitably leads to decreased N content in CN_x [22], which is not desirable for the practical applications of CN_x. Moreover, the addition of N-containing precursor in N-free precursor significantly suppresses the growth of CN_x and results in a dramatically decreased yield [23,24], which makes it difficult to produce CN_x on a large scale.

In this work, CN_x with controlled N doping, tunable structure and high yield have been prepared by ultrasonic spray pyrolysis. The solution used for the synthesis of CN_x consists of a liquid N precursor (acetonitrile) and a solid N precursor (imidazole), acting as the solvent and the solute respectively. The use of this kind of solution avoids the decrease of N content in CN_x, because both components are N-containing precursors. And it is reported that imidazole can produce CN_x with an N content as high as 25.7 at.% [25]. Therefore, it is expected that the addition of imidazole in acetonitrile will increase the N doping in CN_x.

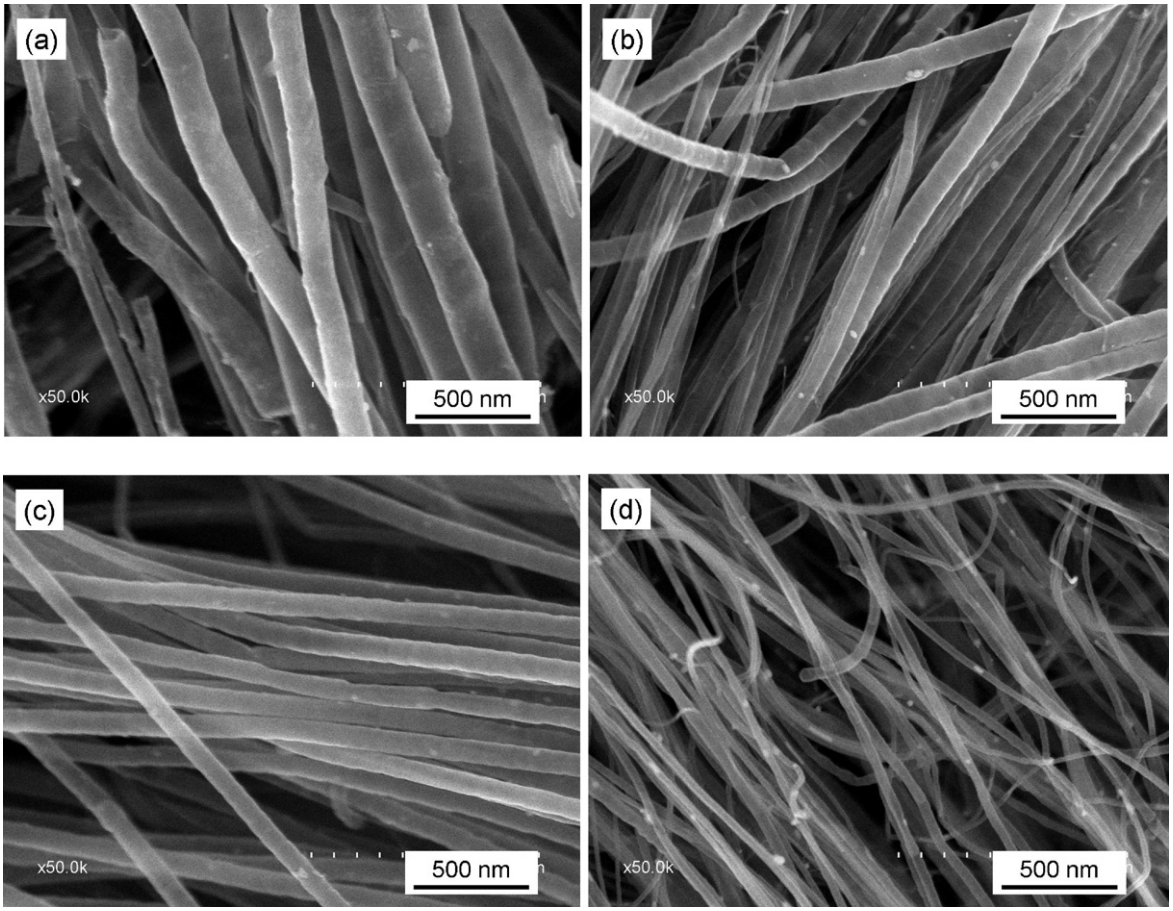

Fig. 2. SEM images of CN_x produced from solutions with different imidazole concentrations: (a) 0 mg/ml; (b) 50 mg/ml; (c) 100 mg/ml; (d) 200 mg/ml. (Solution injection rate 0.25 ml/min; amplitude 45%).

Table 1
Variation of mean nanotube diameter, nanotube length, growth rate and yield of CN_x produced from solutions with different imidazole concentrations.

Imidazole concentration (mg/ml)	Mean nanotube diameter (nm)	Mean nanotube length (μm)	Growth rate (μm/min)	Yield (mg/6ml)
0	89 ± 5	78 ± 8	3.3	12
50	70 ± 4	112 ± 12	4.7	24
100	66 ± 4	154 ± 9	6.4	60
200	54 ± 3	397 ± 18	16.5	192

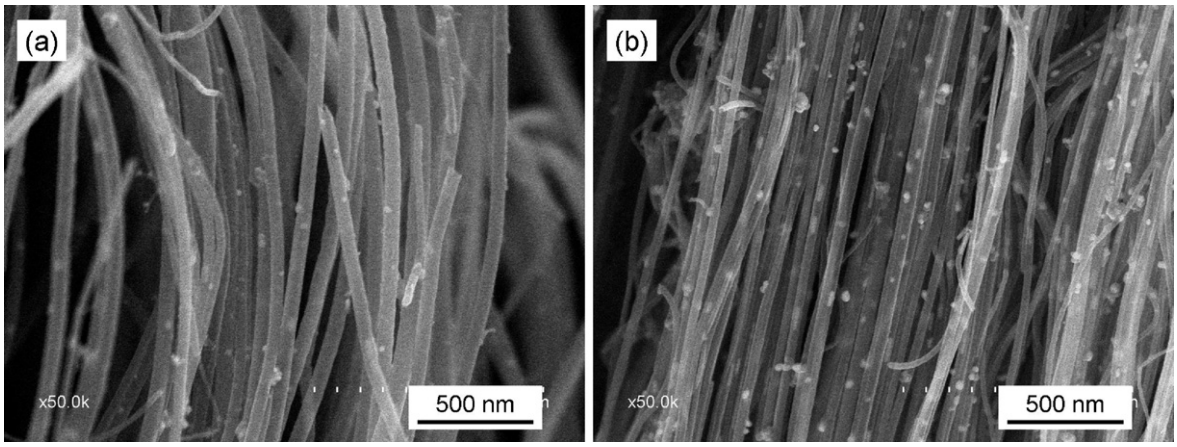

Fig. 3. SEM images of CN_x produced at different solution injection rates (a) 0.5 ml/min; (b) 0.75 ml/min. (Imidazole concentration: 200 mg/ml; amplitude 45%).

2. Experimental method

Fig. 1 shows the schematic illustration of ultrasonic spray pyrolysis. This setup mainly consists of three parts called the injection part, the ultrasonic part, and the deposition chamber. In the injection part, the solution stored in a syringe is injected into the ultrasonic part at a certain feeding rate, which can be precisely controlled on the syringe control panel. In the ultrasonic part, the solution fed by the injection part is atomized in an ultrasonic processor (VCX 130 PB, Sonics & Materials Inc.), and sprayed out as tiny droplets into the deposition chamber. Ultrasonic frequency of the solution can be controlled on the control panel of the ultrasonic processor. The deposition chamber consists of a vertical electrical furnace (50 cm length), a quartz tube (Ø 2.2 cm × 70 cm) with two gas inlets at the top and one gas outlet at the bottom, and a quartz plate (1 mm × 20 mm × 90 mm) attached on a substrate support as the substrate for the growth of CN_x. Once sprayed out by the ultrasonic processor, the solution droplets will be carried by argon (Ar) gas into the center of the furnace, where the pyrolysis occurs.

In a typical process, different amounts (0.5, 1 and 2 g) of imidazole ($C_3H_4N_2$, Alfa Aesar 99%) and 200 mg of ferrocene ($Fe(C_5H_5)_2$, Aldrich 98%) were added into 10 ml of acetonitrile (CH_3CN, 99.5+%), and the mixture was put into an ultrasonic cleaner for 10 min to obtain a homogeneous solution. The solution was then transferred into the syringe in the injection part. The quartz plate used as the substrate for the growth of CN_x was placed in the center of the furnace, with the help of the substrate support. Before the furnace was heated, Ar (99.999% in purity) gas was introduced into the deposition chamber from both inlets for 20 min, and the Ar gas flow rate at each inlet was maintained at 150 sccm. Then the furnace was heated to 850 °C at a rate of 60 °C/min. Once the furnace reached the desirable temperature, 6 ml of the solution prepared as above was injected into the ultrasonic processor at different injection rates (0.25, 0.5 and 0.75 ml/min), and sprayed out as tiny droplets by the ultrasonic processor at different amplitudes (45% and 85%). Then those droplets were carried into the center of the furnace, where the growth of CN_x occurred. After 6 ml of the solution was injected, the furnace was turned off and the system cooled down to room temperature in the flowing Ar gas. CN_x were collected from the quartz plate for future analysis.

The CN_x were characterized by various analysis techniques including Hitachi S-4800 field-emission scanning electron microscopy (SEM) operated at 5 kV, Philips CM 10 transmission electron microscopy (TEM) operated at 80 kV, Kratos Axis Ultra Al (alpha) X-ray photoelectron spectroscopy (XPS) operated at 14 kV, and a HORIBA Scientific LabRAM HR Raman spectrometer operated with an incident laser beam at 532.03 nm.

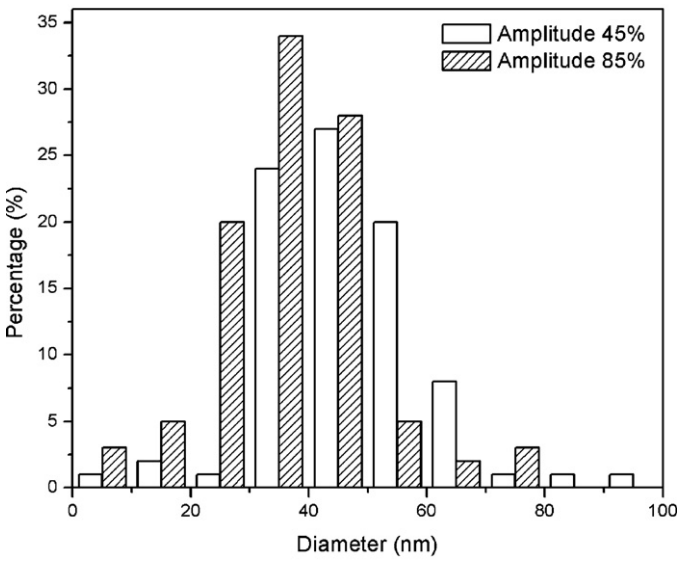

Fig. 4. Diameter distribution of CN_x produced at different ultrasonic amplitudes. (Imidazole concentration: 200 mg/ml; solution injection rate: 0.25 ml/min).

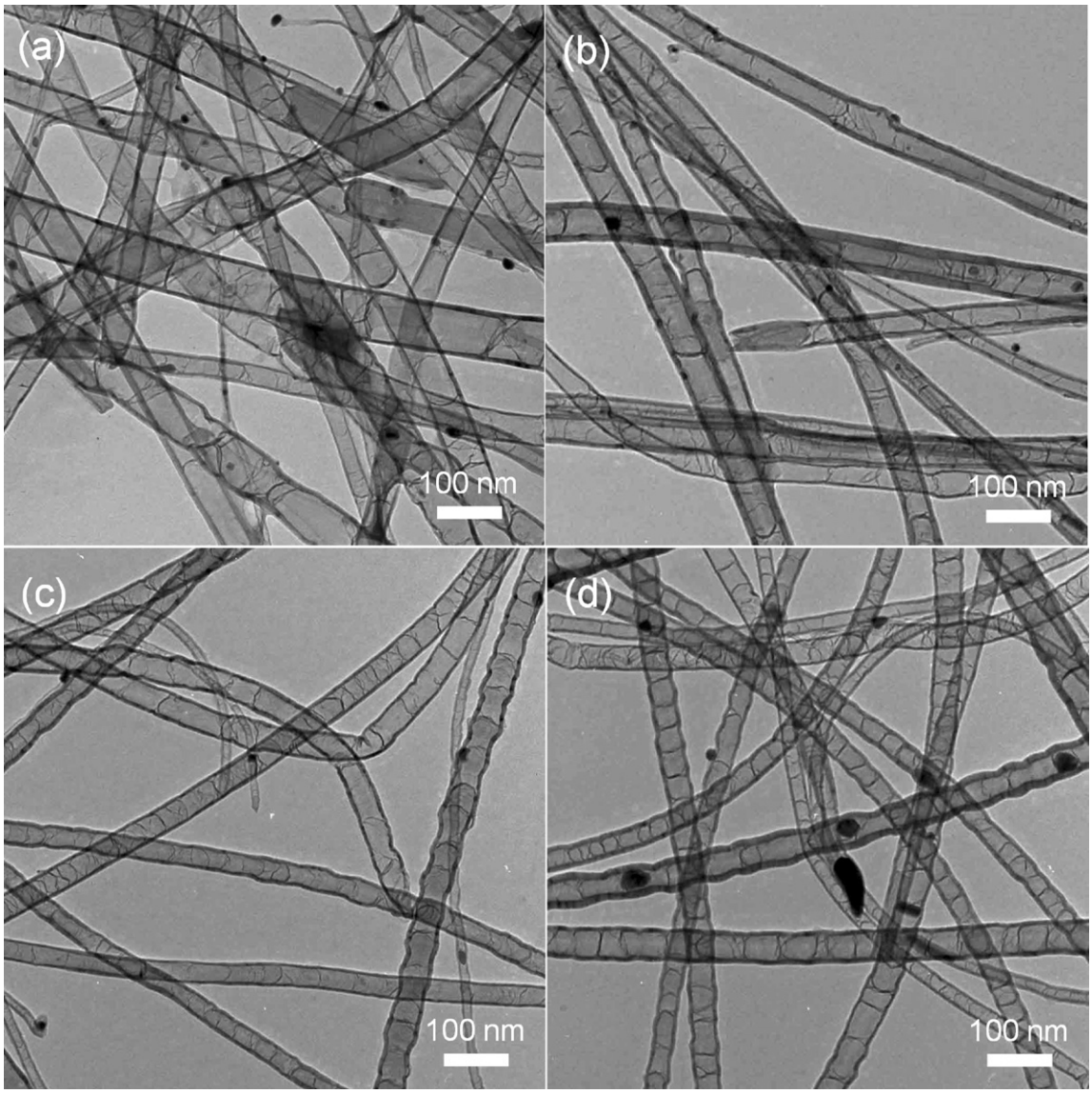

Fig. 5. TEM images of CN_x produced from solutions with different imidazole concentrations: (a) 0 mg/ml; (b) 50 mg/ml; (c) 100 mg/ml; (d) 200 mg/ml. (Solution injection rate 0.25 ml/min; amplitude 45%).

3. Results and discussion

3.1. Morphological investigation by SEM

3.1.1. Effect of imidazole concentration

The effect of imidazole concentration on the growth of CN_x is studied in terms of the nanotube diameter, nanotube length, growth rate and yield. Fig. 2 shows the SEM images of CN_x prepared from solutions with different imidazole concentrations. It can be seen that the nanotube diameter of CN_x changes with the variation of the imidazole concentration. With the increase of the imidazole concentration, the nanotube diameter of CN_x gradually decreases. The diameters of at least 150 nanotubes were measured on TEM images of each sample. Based on these data, their mean diameters are calculated and compared in Table 1. In Table 1, it can be found that when the imidazole concentration increases from 0 to 50, 100 and 200 mg/ml, the mean diameter of CN_x gradually decreases from 89 to 70, 66 and 54 nm, respectively. It is noteworthy that a narrower distribution of diameters can be achieved by increasing imidazole concentration. Koós et al. [22,23] reported that a reduction of nanotube diameter was observed by increasing benzylamine (N-containing precursor) concentration in toluene (N-free precursor). A theoretical calculation [26] shows that the reduced nanotube diameter is mainly due to the presence of N in CN_x, which prefers to stay on the tube edge and thus induces the closure of the nanotubes. This is in accordance with our result. As shown in Section 3.3, the addition of imidazole into acetonitrile leads to the incorporation of more N atoms into CN_x, which is accompanied by the reduction of nanotube diameters.

The nanotube length of each sample was measured, and the results are listed in Table 1. In Table 1, it can be seen that the nanotube length of CN_x is greatly increased with the addition of imidazole. Without imidazole, the nanotube length of CN_x produced in 24 min is measured to be ~78 μm. With 200 mg/ml imidazole, the length of CN_x is found to be ~397 μm. Thus, the growth rate of CN_x is increased from 3.3 μm/min for CN_x prepared without imidazole to 4.7, 6.4, and 16.5 μm/min for CN_x obtained with 50, 100, and 200 mg/ml imidazole, respectively. Consequently, the yield of CN_x is increased with the addition of imidazole, as seen in Table 1. The yield of CN_x was obtained from the product scratched off from the quartz plate. With 200 mg/ml imidazole, 192 mg high-quality CN_x can be easily produced in 24 min. In comparison, the yield of

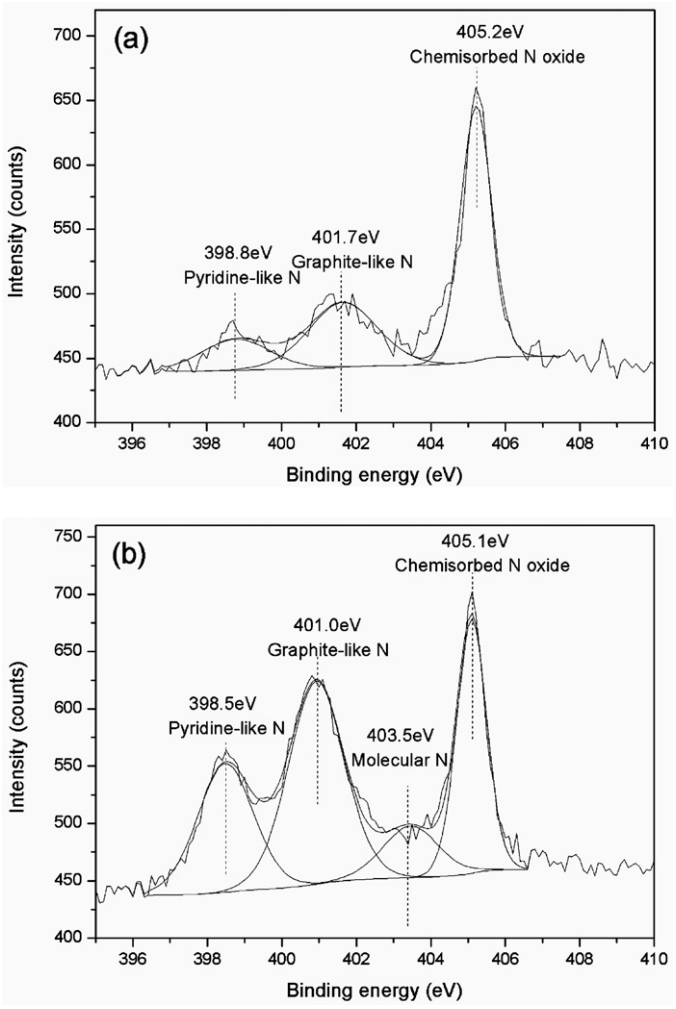

Fig. 6. XPS N 1s spectrum of CN_x produced from solutions with different imidazole concentrations: (a) 0 mg/ml and (b) 200 mg/ml.

CN_x prepared without imidazole in 24 min is only 12 mg, which is only one fifteenth of the former. Therefore, it can be concluded that the addition of imidazole in acetonitrile promotes the growth of nanotubes, and leads to an increased nanotube length and yield for CN_x. Because imidazole can generate high quantities of C–N fragments at 850 °C [25], the solution with imidazole can provide more C–N units than that without imidazole for the growth of the nanotubes. Thus it is reasonable that the addition of imidazole in acetonitrile promotes the growth of CN_x by providing more C–N sources. The trend of nanotube yield in our case is different from previous studies [23,24], in which the addition of an N containing precursor in an N-free precursor leaded to suppressed growth of CN_x. The difference is due to the different solvents used in the solution. The solvent used in our case is an N containing precursor (acetonitrile), while the solvents used in other studies are N-free precursors. It is suggested that pre-existing C–N bonds in the precursor play a key role for the incorporation of N atoms in CN_x [27]. In our case, both imidazole and acetonitrile contain C–N bonds. Therefore, it is reasonable that the doping of N atoms and growth of CN_x would be easier by using the mixture of imidazole and acetonitrile than using a mixture of one N containing precursor and one N-free precursor.

3.1.2. Effect of solution injection rate

The effect of solution injection rate on the growth of CN_x is studied by using a solution with imidazole concentration of 200 mg/ml, and the result is shown in Fig. 3. In Fig. 3, it can be seen that CN_x prepared at solution injection rates of 0.5 and 0.75 ml/min show similarity in the nanotube diameter, which is slightly larger than that of CN_x prepared at 0.25 ml/min, as seen in Fig. 2(d). For CN_x prepared at a solution injection rate of 0.75 ml/min, there are many small catalyst particles attached to the surface of nanotubes. This is due to that only part of the catalyst can catalyze the growth of CN_x at the high solution injection rate. Then the excess catalyst will deposit on the surface of CN_x, forming small catalyst particles. Therefore, the solution injection rate mainly affects the quality of CN_x.

3.1.3. Effect of amplitude

The amplitude of the ultrasonic processor is the last parameter investigated in our study. A solution with 200 mg/ml imidazole was used to grow CN_x at amplitude 45% and 85%. The diameter distribution of each kind of CN_x is shown in Fig. 4. It can be seen that the nanotube diameter of CN_x trends to decrease from 30–60 to 20–50 nm, as amplitude increases from 45% to 85%. The nanotube diameter is usually related to the size of the solution droplet [19]. Higher amplitude of ultrasonic processor can generate solution droplets with smaller sizes, which lead to smaller nanotube diameters. Therefore, the amplitude has an influence on the distribution of the nanotube diameter for CN_x prepared by ultrasonic spray pyrolysis.

3.2. Structural investigation by TEM

The internal structures of CN_x prepared from solutions with different imidazole concentrations are investigated by TEM, and their typical TEM images are shown in Fig. 5. In Fig. 5(a), it can be seen that without imidazole, the produced CN_x have large nanotube diameters and thin nanotube walls. There exist a few interlinks in the internal nanotubes. With the addition of 50 mg/ml imidazole, the nanotube diameter of the prepared CN_x becomes smaller, and interlinks in the nanotubes become denser than that of CN_x synthesized without imidazole, as seen in Fig. 5(b). When the imidazole concentration is further increased to 100 mg/ml, the obtained CN_x show similar internal structure with those prepared with 50 mg/ml imidazole. But their nanotube diameters are slightly decreased. In Fig. 5(d), the nanotubes of CN_x produced with 200 mg/ml imidazole show stacked-cone structure with periodic compartment separation, which is usually called bamboo-like structure. Comparing Fig. 5(a–d), it can be found that the addition of imidazole leads to the formation of a dense bamboo-like structure in the internal nanotubes of CN_x. It is widely accepted that the formation of bamboo-like structure is caused by the presence of N in the graphitic network in CN_x, which induces curvature of the graphitic layer [28,29]. A higher content of N doping usually leads to a denser bamboo-like structure in the internal nanotubes of CN_x [22,23,28]. In our case, the added imidazole generates many C–N fragments during the synthesis process, which introduces more N atoms into CN_x (proved by XPS result in Section 3.3). The doping of more N atoms in CN_x eventually promotes the formation of the denser bamboo-like structure in CN_x by inducing curvature of the graphitic layer. The TEM results suggest that the inner structure of CN_x can be controlled by simply adjusting the imidazole concentration in the solution.

3.3. Content and bonding environment of N by XPS

The content and the bonding environment of N are important factors that determine the properties of CN_x. In order to identify the effect of imidazole on the content and the bonding environment of N doping in CN_x, XPS analysis was carried out on CN_x prepared without imidazole and with 200 mg/ml imidazole, and the results

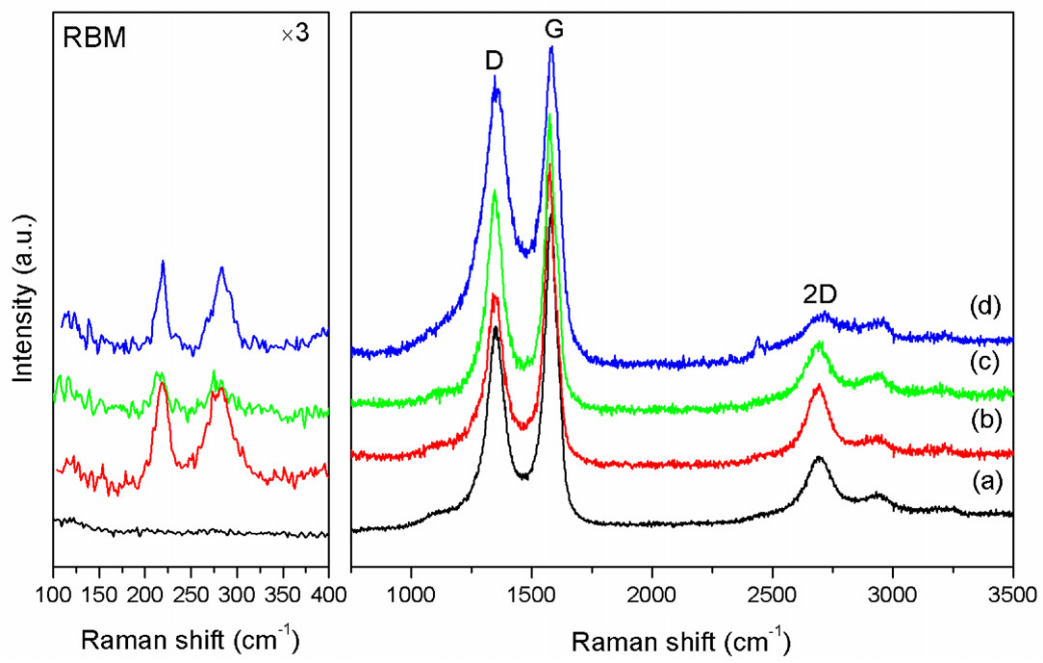

Fig. 7. Raman spectra of CN_x produced from solutions with different imidazole concentrations: (a) 0 mg/ml; (b) 50 mg/ml; (c) 100 mg/ml; (d) 200 mg/ml. (Solution injection rate 0.25 ml/min; amplitude 45%).

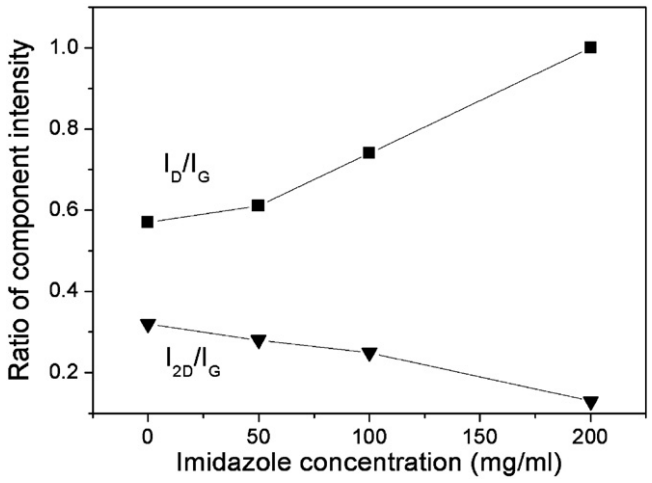

Fig. 8. Integrated intensity ratio of D to G bands (I_D/I_G) and 2D and G band (I_{2D}/I_G) as a function of the imidazole concentration.

are compared in Table 2 and Fig. 6. The N content, defined as atomic percent of N/(C + N), is estimated by the area ratio between the N peak and the sum of N and C peaks. As seen in Table 2, the N content increases from 3.2 at.% for CN_x prepared without imidazole to 5.2 at.% for CN_x prepared with 200 mg/ml imidazole. The XPS N 1s spectra of both samples are fitted into three or four components located at 398.5–398.8, 401.0–401.7, 403.5 (if applicable) and 405.1–405.2 eV, corresponding to pyridine-like N, graphite-like N, molecular N and chemisorbed N oxide, respectively [28], as seen in Fig. 6. The content of each kind of N is calculated and listed in Table 2. In Table 2, it can be seen that the contents of pyridine-like N and graphite-like N are obviously increased for CN_x produced with the addition of imidazole. The intensity ratio between pyridine-like N and graphite-like N (I_{pN}/I_{gN}) is found to increase from 0.48 for CN_x without imidazole to 0.63 for CN_x with 200 mg/ml imidazole. It is noteworthy that molecular N appears in CN_x obtained with 200 mg/ml imidazole. Previous studies have indicated that molecular N can be encapsulated inside the tubes [29,30], or exist as intercalated form between the graphite layers during the growth of CN_x [31]. The content of chemisorbed N oxide is slightly decreased for CN_x obtained with 200 mg/ml imidazole, compared with those produced without imidazole. Therefore, the addition of imidazole not only increases the N content in CN_x, but also alters bonding environments of N in CN_x.

3.4. Crystallinity of CN_x by Raman spectra

To obtain the information on the crystallinity of CN_x, Raman spectra were carried out on CN_x prepared with different imidazole concentrations, and their spectra are compared in Fig. 7. From Fig. 7, it can be seen that the Raman spectra show two main peaks around 1350 and 1590 cm^{-1}, corresponding to the D-band and the G-band respectively. The D-band is originated from atomic displacement and disorder induced features caused by lattice defect, distortion or the finite particle size [32], while the G-band indicates the formation of well-graphitized carbon nanotubes [33]. A second-order peak located at ~2700 cm^{-1} is also observed and usually named

Table 2
Total N content and contents of different types of N in CN_x produced from solutions with imidazole concentration of 0 and 200 mg/ml.

Imidazole concentration (mg/ml)	N content (at.%)				
	Total	Pyridine-like N	Graphite-like N	Molecular N	Chemisorbed N oxide
0	3.2	0.47	0.97	–	1.76
200	5.2	1.28	2.03	0.51	1.36

2D-band, and the 2D-band is an overtone mode of the D-band [34]. Previous studies [23,28,34] have shown that N doping in CN_x usually increases the intensity of D-band while decreases the intensity of 2D-band, due to increased defect density in the nanotubes. In our case, the increase of imidazole concentration in acetonitrile leads to an increase of the intensity of D-band and a decrease of the intensity of 2D-band. The intensity ratios of D to G and 2D to G are calculated to quantitatively show this variation, as shown in Fig. 8. As the imidazole concentration increases from 0 to 50, 100 and 200 mg/ml, the D/G ratio gradually increases from 0.57 to 0.61, 0.74 and 1, respectively. Meanwhile, 2D/G ratio decreases from 0.32 to 0.28, 0.25 and 0.13.The Raman results indicate that the addition of imidazole induces an increase in the defects and disorder in CN_x. The reason could be attributed to the doping of more N atoms in CN_x with the addition of imidazole.

It is interesting to note that the Raman spectra of CN_x prepared with imidazole show radial breathing mode (RBM) between 180 and 280 cm^{-1}, which is the fingerprint of single-wall carbon nanotubes (SWNTs) [35]. The corresponding diameter of SWNTs is estimated in the range of 0.9–1.1 nm, by using the empirical relation $d\,(nm) = 248/\nu\,(cm^{-1})$, where d is the SWNTs diameter and ν is Raman shift [35,36]. The appearance of SWNTs in CN_x is partially due to the decrease of nanotube diameters with the addition of imidazole in the solution. Another possible reason is the secondary generation of nanotubes during the synthesis process [22,37]. During the synthesis process, the surface of the quartz plate was totally covered by nanotubes within a few minutes. Then incoming catalyst could not reach the quartz plate, and would deposit on the nanotube surface for the growth of CN_x [22,37]. These new catalyst particles grown on the nanotube surface were much smaller than those grown on the surface of the quartz plate [37], and this increase the possibility of the appearance of SWNTs. Moreover, CN_x with higher N content have more active nanotube surface, which would be easier for the deposition of catalyst particles. Thus, CN_x with a high N content have more chance for the appearance of SWNTs than those with a low N content. This would explain why that SWNTs did not appear in CN_x prepared without imidazole. Therefore, ultrasonic spray pyrolysis also shows the potential in the synthesis of N doped SWNTs. Large amounts of N doped SWNTs are expected when the catalyst concentration is decreased in the solution.

4. Conclusions

Ultrasonic spray pyrolysis was developed to synthesize nitrogen-doped carbon nanotubes (CN_x) from mixtures of acetonitrile and imidazole. A systematic study was carried out on the effect of solution injection rate, amplitude of the ultrasonic processor and imidazole concentration on the growth of CN_x. The results showed that the solution injection rate mainly affected the quality of CN_x, and the amplitude had an influence on the diameter distribution of CN_x. SEM and TEM studies indicated that the increase of imidazole concentration decreased the nanotube diameter, while increased the nanotube length and the density of bamboo-like structure in CN_x. XPS and Raman spectra analysis showed that the addition of imidazole promoted the N doping and introduced more defects in CN_x. These results suggest that by simply adjusting the imidazole concentration in acetonitrile, it is possible to control the nanotube diameter and length, internal structure, N content and defect density in CN_x produced by ultrasonic spray pyrolysis.

Acknowledgements

This research was supported by Natural Sciences and Engineering Research Council of Canada (NSERC), Canada Research Chair (CRC) Program, Canada Fundation for Innovation (CFI), Ontario Research Fund (ORF), Ontario Early Researcher Award (ERA) and University of Western Ontario.

References

[1] S. Iijima, Helical microtubules of graphitic carbon, Nature 354 (1991) 56–58.
[2] R.H. Baughman, A.A. Zakhidov, W.A. De Heer, Carbon nanotubes-the route toward applications, Science 297 (2002) 787–792.
[3] D. Villers, S.H. Sun, A.M. Serventi, J.P. Dodelet, S. Desilets, Characterization of Pt nanoparticles deposited onto carbon nanotubes grown on carbon paper and evaluation of this electrode for the reduction of oxygen, J. Phys. Chem. B 110 (2006) 25916–25925.
[4] P. Ayala, R. Arenal, M. Rümmeli, A. Rubio, T. Pichler, The doping of carbon nanotubes with nitrogen and their potential applications, Carbon 48 (2010) 575–586.
[5] P. Nemes-incze, N. Daróczi, Z. Sárközi, A.A. Koós, K. Kertész, O. Tiprigan, Z.E. Horváth, A.L. Darabont, L.P. Biró, Synthesis of bamboo-structured multiwalled carbon nanotubes by spray pyrolysis method, using a mixture of benzene and pyridine, J. Optoelectron. Adv. Mater. 9 (2007) 1525–1529.
[6] A. Nevidomskyy, G. Csanyi, M. Payne, Chemically active substitutional nitrogen impurity in carbon nanotubes, Phys. Rev. Lett. 91 (2003) 105502–105506.
[7] C. Kaun, B. Larade, H. Mehrez, J. Taylor, H. Guo, Current-voltage characteristics of carbon nanotubes with substitutional nitrogen, Phys. Rev. B 65 (2002) 205416–205421.
[8] E.M.M. Ibrahim, V.O. Khavrus, A. Leonhardt, S. Hampel, S. Oswald, M.H. Rümmeli, B. Büchner, Synthesis, characterization, and electrical properties of nitrogen-doped single-walled carbon nanotubes with different nitrogen content, Diamond Relat. Mater. 19 (2010) 1199–1206.
[9] E. Hernandez, C. Goze, P. Bernier, A. Rubio, Elastic properties of single-wall nanotubes, Appl. Phys. A Mater. Sci. Process. 68 (1999) 287–292.
[10] K. Gong, F. Du, Z. Xia, M. Durstock, L. Dai, Nitrogen-doped carbon nanotube arrays with high electrocatalytic activity for oxygen reduction, Science 323 (2009) 760–764.
[11] S.K. Srivastava, V.D. Vankar, D.V. Sridhar Rao, V. Kumar, Enhanced field emission characteristics of nitrogen-doped carbon nanotube films grown by microwave plasma enhanced chemical vapor deposition process, Thin Solid Films 515 (2006) 1851–1856.
[12] K. Ghosh, M. Kumar, T. Maruyama, Y. Ando, Tailoring the field emission property of nitrogen-doped carbon nanotubes by controlling the graphitic/pyridinic substitution, Carbon 48 (2010) 191–200.
[13] Y. Chen, J. Wang, H. Liu, R. Li, X. Sun, S. Ye, S. Knights, Enhanced stability of Pt electrocatalysts by nitrogen doping in CNTs for PEM fuel cells, Electrochem. Commun. 11 (2009) 2071–2076.
[14] Y. Chen, J. Wang, H. Liu, M.N. Banis, R. Li, X. Sun, T.-K. Sham, S. Ye, S. Knights, Nitrogen doping effects on carbon nanotubes and the origin of the enhanced electrocatalytic activity of supported Pt for proton-exchange membrane fuel cells, J. Phys. Chem. C 115 (2011) 3769–3776.
[15] M. Glerup, J. Steinmetz, D. Samaille, O. Stephan, S. Enouz, A. Loiseau, S. Roth, P. Bernier, Synthesis of N-doped SWNT using the arc-discharge procedure, Chem. Phys. Lett. 387 (2004) 193–197.
[16] H. Liu, R. Arenal, S. Enouz-Vedrenne, O. Stephan, A. Loiseau, Nitrogen Configuration in Individual CNx-SWNTs Synthesized by Laser Vaporization Technique, J. Phys. Chem. C 113 (2009) 9509–9511.
[17] M. He, S. Zhou, J. Zhang, Z. Liu, C. Robinson, CVD growth of N-doped carbon nanotubes on silicon substrates and its mechanism, J. Phys. Chem. B 109 (2005) 9275–9279.
[18] M.I. Ionescu, Y. Zhang, R. Li, X. Sun, H. Abou-Rachid, L.-S. Lussier, Hydrogen-free spray pyrolysis chemical vapor deposition method for the carbon nanotube growth: parametric studies, Appl. Surf. Sci. (2010), doi:10.1016/j.apsusc.2011.03.011.
[19] A. Barreiro, D. Selbmann, T. Pichler, K. Biedermann, M.H. Rümmeli, U. Schwalke, B. Büchner, On the effects of solution and reaction parameters for the aerosol-assisted CVD growth of long carbon nanotubes, Appl. Phys. A: Mater. Sci. 82 (2006) 719–725.
[20] C. Tang, Y. Bando, D. Golberg, D. Xu, Structure and nitrogen incorporation of carbon nanotubes synthesized by catalytic pyrolysis of dimethylformamide, Carbon 42 (2004) 2625–2633.
[21] E. Xu, J. Wei, K. Wang, Z. Li, X. Gui, Y. Jia, H. Zhu, D. Wu, Doped carbon nanotube array with a gradient of nitrogen concentration, Carbon 48 (2010) 3097–3102.
[22] A.A. Koós, M. Dowling, K. Jurkschat, A. Crossley, N. Grobert, Effect of the experimental parameters on the structure of nitrogen-doped carbon nanotubes produced by aerosol chemical vapor deposition, Carbon 47 (2009) 30–37.
[23] A.A. Koós, F. Dillon, E.A. Obraztsova, A. Crossley, N. Grobert, Comparison of structural changes in nitrogen and boron-doped multi-walled carbon nanotubes, Carbon 48 (2010) 3033–3041.
[24] E.N. Nxumalo, P.J. Letsoalo, L.M. Cele, N.J. Coville, The influence of nitrogen sources on nitrogen doped multi-walled carbon nanotubes, J. Organomet. Chem. 695 (2010) 2596–2602.
[25] K. Ghosh, M. Kumar, T. Maruyama, Y. Ando, Controllable growth of highly N-doped carbon nanotubes from imidazole: structural, spectroscopic and field emission study, J. Mater. Chem. 20 (2010) 4128–4134.
[26] B.G. Sumpter, V. Meunier, J.M. Romo-Herrera, E. Cruz-Silva, D.A. Cullen, H. Terrones, D.J. Smith, M. Terrones, Nitrogen-mediated carbon nanotube growth: diameter reduction, metallicity, bundle dispersability, and bamboo-like structure formation, ACS Nano 1 (2007) 369–375.

[27] C Tang, Y. Bando, D. Golberg, F. Xu, Structure and nitrogen incorporation of carbon nanotubes synthesized by catalytic pyrolysis of dimethylformamide, Carbon 42 (2004) 2625–2633.
[28] H. Liu, Y. Zhang, R. Li, X. Sun, S. Désilets, H. Abou-Rachid, M. Jaidann, L.-S. Lussier, Structural and morphological control of aligned nitrogen-doped carbon nanotubes, Carbon 48 (2010) 1498–1507.
[29] M. Reyes-Reyes, N. Grobert, R. Kamalakaran, T. Seeger, D. Golberg, M. Rühle, Y. Bando, H. Terrones, M. Terrones, Efficient encapsulation of gaseous nitrogen inside carbon nanotubes with bamboo-like structure using aerosol thermolysis, Chem. Phys. Lett. 396 (2004) 167–173.
[30] H.C. Choi, S.Y. Bae, W.S. Jang, J. Park, Release of N_2 from the carbon nanotubes via high-temperature annealing, J. Phys. Chem. B 109 (2005) 1683–1688.
[31] H.C. Choi, S.Y. Bae, J. Park, Experimental and theoretical studies on the structure of N-doped carbon nanotubes: possibility of intercalated molecular N_2, Appl. Phys. Lett. 85 (2004) 5742–5744.
[32] H. Choi, J. Park, B. Kim, Distribution and structure of N atoms in multiwalled carbon nanotubes using variable-energy X-ray photoelectron spectroscopy, J. Phys. Chem. B 109 (2005) 4333–4340.
[33] M.S. Dresselhaus, G. Dresselhaus, R. Saito, A. Jorio, Raman spectroscopy of carbon nanotubes, Phys. Rep. 409 (2005) 47–99.
[34] L.G. Bulusheva, A.V. Okotrub, I.A. Kinloch, I.P. Asanov, A.G. Kurenya, A.G. Kudashov, X. Chen, H. Song, Effect of nitrogen doping on Raman spectra of multi-walled carbon nanotubes, Phys. Status Solidi (b) 245 (2008) 1971–1974.
[35] I. Khatri, T. Soga, T. Jimbo, S. Adhikari, H.R. Aryal, M. Umeno, Synthesis of single walled carbon nanotubes by ultrasonic spray pyrolysis method, Diamond Relat. Mater. 18 (2009) 319–323.
[36] S. Chaisitsak, J. Nukeaw, A. Tuantranont, Parametric study of atmospheric-pressure single-walled carbon nanotubes growth by ferrocene-ethanol mist CVD, Diamond Relat. Mater. 16 (2007) 1958–1966.
[37] C. Singh, M. Shaffer, A. Windle, Production of controlled architectures of aligned carbon nanotubes by an injection chemical vapor deposition method, Carbon 41 (2003) 359–368.